Solar Physics (2022) 297:24
https://doi.org/10.1007/s11207-022-01951-4

Check for updates

Precursory Signals of Forbush Decreases Not Connected with Shock Waves

D. Lingri[1] · H. Mavromichalaki[1] · M. Abunina[2] · A. Belov[2] · E. Eroshenko[2] · I. Daglis[1,3] · A. Abunin[2]

Received: 2 January 2021 / Accepted: 19 January 2022

Abstract
Forbush decreases (FDs) are sharp reductions of the cosmic-ray (CR) intensity, following intense solar activity such as coronal mass ejections (CMEs) and their corresponding interplanetary shocks. In some cases, shocks create sudden storm commencements (SSCs) at the Earth's magnetosphere with significant interest for space-weather studies. Preincreases and/or predecreases of CR intensity before the onset of FDs, known as precursory signals, have been widely examined by many authors. In this work, an attempt to define precursory signals that are not related to SSCs is presented. For the present analysis, CR data recorded by the ground-based *Neutron Monitor Network* as well as data on solar flares, CMEs, solar-wind speed, interplanetary magnetic field, and geomagnetic indices for the years 1969 – 2019 are used. To identify FDs that present precursors, the adopted criteria are mainly the FD amplitude ($> 2\%$) and the equatorial CR anisotropy before the onset time ($> 0.8\%$). The analysis of FDs and the study of their asymptotic-longitude CR distribution for precursors are based on the *Global Survey Method* and the *Ring of Stations Method*, respectively. Precursory signals are identified in 17 out of 27 events without SSCs.

Keywords Solar activity · Cosmic rays · Neutron monitor · Forbush decreases · Precursors

1. Introduction

Galactic cosmic rays (GCRs) are energetic particles modulated by the Sun and heliosphere, and they present great variability. Sudden depressions of these particles followed by a gradual recovery phase of about one week, the so-called Forbush decreases (FDs), are often recorded inside the heliosphere (Forbush, 1938, 1954; Lockwood, 1971; Cane, 2000). FDs are mostly generated by solar-eruption events, such as coronal mass ejections that expand and propagate through the interplanetary medium and arrive at the Earth's magnetosphere

✉ H. Mavromichalaki
emavromi@phys.uoa.gr

1 Department of Physics, National and Kapodistrian University of Athens, Athens, Greece

2 Pushkov Institute of Terrestrial Magnetism, Ionosphere and Radio Wave Propagation of the Russian Academy of Sciences (IZMIRAN), Troitsk, Moscow, Russia

3 Hellenic Space Center, Athens, Greece

Published online: 23 February 2022

(Russell and Mulligan, 2002; Janvier et al., 2019). Interplanetary coronal mass ejections (ICMEs), which can create an interplanetary shock, compress the magnetosphere, and produce a sudden storm commencement (SSC) (Cane, 2000; Dumbović et al., 2019). The Earth's position in the heliosphere, combined with the Parker spiral of the solar magnetic field in the interplanetary medium, determine the existence of an SSC (Hofer and Fluckiger, 2000). FDs without SSC association present a more symmetrical and smoother profile, while in most cases, they have a smaller amplitude than those associated with SSC (Belov, 2008; Melkumyan et al., 2019).

Sometimes, the onset of FDs coincides with the detection of an SSC (Papailiou et al., 2012a; Lingri et al., 2019; Melkumyan et al., 2021). When an interplanetary disturbance is registered, the interplanetary magnetic-field intensity (IMF) and/or the solar-wind speed often increase. Thus, the onset of FDs without SSC can be defined by the sharp increase of the IMF (e.g. Richardson, 2004; Abunina et al., 2020) and/or of the solar-wind velocity (Iucci et al., 1979). It cannot be defined by isolated ground-based neutron monitors (NMs), as FDs are not recorded worldwide simultaneously (e.g. Belov, 2008; Okike and Collier, 2011).

Before the onset of the FD main phase and when the solar disturbance reaches the Earth, significant changes in cosmic-ray (CR) anisotropy are observed and while the precursor of the approaching disturbance in the CR anisotropy has a complex shape, the first harmonic of the solar-diurnal anisotropy is increased (Jacklyn, Duggal, and Pomerantz, 1969; Papailiou et al., 2012a). Then precursory signals, such as preincreases and/or predecreases of the CR intensity, may appear, which is useful for the prediction of the upcoming event (e.g. Lockwood, 1971; Nagashima et al., 1993; Belov et al., 1995; Ruffolo et al., 1999; Dorman, 2005; Kudela and Storini, 2006; Papailiou et al., 2012a; Lingri et al., 2016; Tortermpun, Ruffolo, and Bieber, 2018). These precursors in CR intensity can be observed in a time range between 2 to 20 hours before the onset of the FD (Asipenka et al., 2009; Papailiou et al., 2012b; Lingri et al., 2019). Observations of the CR anisotropy are crucial for the early detection of FD precursors, using CR data from NMs. When NMs are magnetically connected with low-density areas of CRs upstream of the upcoming disturbance, known as the "loss cone" effect, a predecrease is recorded in CR data (Leerungnavarat, Ruffolo, and Bieber, 2003; Papailiou et al., 2013; Lingri et al., 2019 and references therein). On the other hand, the front of the stream reflects and accelerates CR particles, which are recorded by NMs as a preincrease (Dorman et al., 1995; Belov et al., 1995; Kudela and Storini, 2006).

Most published studies are focused on cases of FDs accompanied by interplanetary shocks recorded by spacecraft (Belov et al., 1995; Ruffolo et al., 1999; Leerungnavarat, Ruffolo, and Bieber, 2003; Papailiou et al., 2013; Lingri et al., 2019). The main question here is whether a precursory signal could also be observed in events that are not generated by a shock. It was recently opined that FDs without shock association may also have precursory signals (Abunina et al., 2020).

The aim of this study is to find FD events without SSC that present precursory signals. The selection of the examined events is based on the *Forbush Effects and Interplanetary Disturbances Database* (FEID). The existence of precursor signs before the onset of the selected events has been examined using the *Ring of Stations Method* (RSM). This method is described in Section 2. The determination of the adopted criteria for the selection of the events examined and the study for precursors are presented in Sections 3 and 4, respectively. Results and discussion as well as a comparative study of the precursory characteristics of the FDs studied here with those with SSC association for Solar Cycle 24 are presented in Section 5.

2. Data and Methods

Starting from Climax, Colorado (USA) in the 1950s (Simpson, 2000), more and more NM stations were constructed all over the world, creating a worldwide NM network that nowadays numbers about fifty stations in operation. This network makes the comparison of the CR intensity variations recorded by the NMs all over the world easier. The *European High-resolution Real-time Neutron Monitor Database* (NMDB: www.nmdb.eu) provides easy access to all NM measurements that play a key role in space-weather studies and applications (Mavromichalaki et al., 2011).

Since the 1970s, with some gaps around 1985 – 1992, there are also continuous data of the solar wind, simultaneously with observations of the solar disk from the *Geostationary Operational Environmental Satellites* (GOES) (www.ngdc.noaa.gov/stp/space-weather/solar-data/solar-features/solar-flares/x-rays/goes/xrs/). CME data have been retrieved from the SOHO/LASCO CME Catalog (cdaw.gsfc.nasa.gov/CME_list/) of the *Solar and Heliospheric Observatory* (SOHO) and especially from the *Large Angle and Spectrometric Coronagraph* (LASCO).

Data of the solar-wind velocity and the IMF, as well as of the geomagnetic indices Dst and Kp are obtained from the OMNIWeb site (omniweb.gsfc.nasa.gov). The identification of the presence or the absence of an interplanetary shock is based on *Advanced Composition Explorer* (ACE) and/or *Wind* spacecraft data (www.cfa.harvard.edu/shocks/).

The FDs examined here are selected from the FEID database of the Pushkov Institute of Terrestrial Magnetism, Ionosphere, and Radiowave Propagation of the Russian Academy of Sciences (IZMIRAN) (spaceweather.izmiran.ru/eng/dbs.html; Belov et al., 2019). This database includes about 7500 FDs from the year 1957 to date (Abunin et al., 2019). Among them, about 1500 FDs are associated with SSCs, while the rest of them are without an SSC.

The FEID contains a great deal of CR information based on the *Global Survey Method* (GSM) results. However, more detailed information is needed for the present study. The main reason for using GSM is to obtain whole CR time series and not only FD characteristics. The output data used in this work are the CR-density variation [A_o], as well as the three anisotropy components [A_x, A_y, A_z] that are calculated for CRs with cutoff rigidity 10 GV, representative of the effective rigidity of the NMs (Belov et al., 2018). For these calculations, the GSM is applied to the data of the worldwide NM network, considering the characteristics of each NM, such as asymptotic directions, coupling coefficients, yield functions, and others (Asipenka et al., 2009; Belov et al., 2018).

The RSM was also used to search for the possible existence of precursors before the FD event onset. It should be emphasized that the RSM is another way to present raw NM data, as it presents them without corrections and modeling. The CR intensity, as well as the asymptotic directions of particles' arrival at a number of neutron-monitor stations (Table 1), are used to determine the possible precursory signals (Belov et al., 2003; Asipenka et al., 2009; Papailiou et al., 2012b; Lingri et al., 2019; Abunina et al., 2020). A description of the RSM features, applicability, and advantages are presented in detail by Abunina et al. (2020). The large angular dependence is convincingly demonstrated both theoretically (e.g. Ruffolo et al., 1999; Leerungnavarat, Ruffolo, and Bieber, 2003) and experimentally (e.g. Nagashima et al., 1992; Munakata et al., 2000; Belov et al., 2003; Kuwabara et al., 2006) since a FD precursor is an essentially anisotropic phenomenon. Diagrams of asymptotic longitudes, together with data from NMs with specific properties for each event, are plotted. To prepare these plots, hourly averaged CR data, corrected for pressure, are taken from the NMDB (www.nmdb.eu; Mavromichalaki et al., 2011), from the *Network of Cosmic ray Stations* of IZMIRAN (cr0.izmiran.ru) and *World Data Center for Cosmic Rays* of Nagoya

University (cidas.isee.nagoya-u.ac.jp/WDCCR/). The use of all of the above CR databases is necessary due to data gaps (Väisänen, Usoskin, and Mursula, 2021).

It is worth noting that NMs used in the RSM follow the criteria below in order to respond similarly to variations of the CR anisotropy: the cutoff rigidity should be less than or equal to 3 GV and the NM station location should be at an altitude lower than 1000 m. These limitations are to provide directional sensitivity (Kuwabara et al., 2006). The subpolar NM stations are not taken into account, as they are affected by the North–South anisotropy [A_z] (Belov et al., 2017a, 2017b). On average, data from about 18 – 25 NM stations were used for drawing each of the time–longitude distributions. By using as many NMs as possible, a better depiction of the temporal variations of the CR-intensity distribution in asymptotic directions is achieved (Papailiou et al., 2012a; Abunina et al., 2020). A list of the NM stations used along with some of their main characteristics (geographic coordinates, cutoff rigidity, and altitude) is given in Table 1.

It should be noted that, besides RSM, there are other methods for the study of precursors, based on data from individual NMs (Hofer and Fluckiger, 2000; Ahluwalia, Ygbuhay, and Duldig, 2009) and also on the pitch-angle distribution (Kuwabara et al., 2006). An example of FDs as they are recorded by individual stations is given in the next section. The pitch-angle and the asymptotic-longitude distributions, on which RSM is based, are two types of data presentation that are essentially very similar. The pitch-angle distribution is easier to compare with theory, but the longitude distribution is easier to obtain in practice, it is clearer, and it does not depend on IMF data. This is why the pitch-angle distribution is not analyzed in the present study.

3. Selection of Events

The time period under study is from 1969 to 2019, which corresponds to four and a half solar cycles (half of Cycle 20 and Cycles 21, 22, 23, and 24). During this period, more than 6000 FDs have been recorded. Solar-wind and IMF data are also available. In this work, in order to select the events examined, a number of criteria have been adopted and are indicated below:

i) The FDs are **not** associated with an SSC.
ii) The FD amplitude is equal to or greater than 2%.
iii) The maximal reduction is observed in a time frame of about two days after the event onset.
iv) The A_{xy}-component of CR anisotropy one hour before the onset has to be greater than 0.8% [A_{xyb}]. As the mean value of A_{xy} is around 0.52% (Belov et al., 2017a), the value of 0.8% is significantly higher, and it is an indication of the existence of a precursor (Papailiou et al., 2012a).
v) Events that are not accompanied with the simultaneous solar-wind, interplanetary, and CR data, are excluded. Information about the interplanetary environment is necessary to define the onset, identify the solar-source type, and verify shock-wave existence.
vi) If an increased IMF (>10 nT) is recorded for about a day before the event onset, this FD could not be studied for precursors, as the interplanetary medium is characterized as disturbed and the CR variations may be due to another source and not to the upcoming stream.
vii) In this study, events that are reliably identified with solar sources and associated with ICMEs are examined. Events associated with high-speed streams from coronal holes and recurrent FDs are not included.

Table 1 NM stations and their characteristics used in this work.

No	NM stations	Abbr.	Geograph. coordinates		Rigidity [GV]	Altitude [m]
1	Apatity, Russia	APTY	67.57° N	33.40° E	0.65	177
2	Cape Shmidt, Russia	CAPS	68.92° N	179.47° W	0.45	0
3	Deep River, Canada	DPRV	46.10° N	77.50° W	1.14	145
4	Durham, USA	DRHM	43.10° N	70.83° W	1.58	0
5	Fort Smith, Canada	FSMT	60.02° N	111.93° W	0.30	180
6	Goose Bay, Canada	GSBY	53.27° N	60.40° W	0.64	46
7	Inuvik, Canada	INVK	68.36° N	133.72° W	0.30	21
8	Kerguelen, France	KERG	49.35° S	70.25° E	1.14	33
9	Kingston, Australia	KGSN	42.99° S	147.29° E	1.88	65
10	Kiel, Germany	KIEL	54.34° N	10.12° E	2.36	54
11	Larc, Antarctica	LARC	66.20° S	58.96° W	3.00	40
12	Leeds, England	LEED	53.80° N	01.55° W	2.20	72
13	McMurdo, Antarctica	MCMU	77.95° S	166.60° E	0.30	48
14	Mobile CR Laboratory, Russia	MCRL	55.47° N	37.32° E	2.46	200
15	Magadan, Russia	MGDN	60.04° N	151.05° E	2.10	220
16	Moscow, Russia	MOSC	55.47° N	37.32° E	2.43	200
17	Mt. Wellington, Australia	MTWL	42.92° S	147.25° E	1.80	725
18	Mawson, Antarctica	MWSN	67.60° S	62.88° E	0.22	0
19	Nain, Canada	NAIN	56.55° N	61.68° W	0.30	46
20	Newark, USA	NEWK	39.68° N	75.75° W	2.40	50
21	Norilsk, Russia	NRLK	69.26° N	88.05° E	0.63	0
22	Novosibirsk, Russia	NVBK	54.48° N	83.00° E	2.91	163
23	Oulu, Finland	OULU	65.05° N	25.47° E	0.81	15
24	Peawanuk, Canada	PWNK	54.98° N	85.44° W	0.30	53
25	Sanae IV, Antarctica	SNAE	71.40° S	02.51° W	0.73	856
26	Sverdlovsk, Russia	SVER	56.43° N	60.57° E	2.30	300
27	Tixie Bay, Russia	TXBY	71.01° N	128.54° E	0.48	0
28	Utrecht, The Netherlands	UTRT	52.10° N	05.12° E	2.76	0
29	Yakutsk, Russia	YKTK	62.01° N	129.43° E	1.65	105

By following the above restrictions and criteria, 27 events remained under study for precursors. It is noted that in Solar Cycle 22, FDs are not presented, as they are excluded due to the lack of corresponding solar and interplanetary data. A list of the selected events with their characteristics is presented in Table 2. The first column gives the serial number of events, while the second one gives the date and the time of the event onset. The third column provides the FD amplitude at the rigidity of 10 GV, as calculated by the GSM. The fourth and fifth columns provide the maximal geomagnetic indices (Kp and Dst, respectively) during these specific events. The maximum values of IMF and solar-wind velocity are presented in the sixth and seventh columns, respectively. The next column presents the equatorial anisotropy one hour before the onset [A_{xyb}]. The next three columns refer to the possible solar source of the specified event (date/time, class, and coordinates of solar flares). In some cases, we do not choose a flare as a solar source, but a disappeared solar filament

Table 2 FDs studied in this work that presented precursor signals. Superscript I indicates the FDs that are analyzed in this work. With minus (−) are signed predecreases, with plus (+) preincreases, and with plus/minus (±) events with both signals.

S/N	Date/Time YYYY.MM.DD hh:mm	FD ampl. [%]	Kp [nT]	Dst [nT]	IMF [nT]	Vsw [km s^{-1}]	A_{xyb}	Possible solar sources: Date/Time YYYY.MM.DD hh:mm	Possible solar sources: Flare/DSF	Possible solar sources: Coordinates [location]	Precursors Decrease (−) Increase (+)
1	1971.03.23 01:00	2.4	4−	−24	11.6	549	0.89				no
2	1972.11.01 05:00	4.1	6−	−70	17.1	603	0.80				no
3	1975.04.07 15:00	2.1	6	−55	13.7	711	1.01				no
4	1978.12.21 23:00	2.8	4+	−29	14.7	566	1.66				–
5	1979.08.17 16:00	2.4	3+	−11	7.9	440	2.14	1979.08.14 12:43	M3.0	S22E73	±
6	1979.09.17 06:00	6.2	7	−158	18.1	449	1.39				±
7[I]	1980.10.10 21:00	2.7	6	−104	14.0	579	0.88	1980.10.08 20:21	M3.4	S07E65	±
8	1980.11.29 23:00	3.1	5	−64	12.1	557	1.48				±
9	1982.01.13 05:00	2.0	2+	12	11.5	326	2.75	1982.01.08 13:54	M3.0	N10W60	–
10[I]	1999.05.22 20:00	2.7	3+	−2	8.4	489	1.83				–
11	2000.11.22 11:00	3.1	3−	−22	8.6	406	1.12	2000.11.18 13:02	M1.5	N11E37	–
12	2001.04.14 02:00	2.4	4+	−68	10.3	721	1.69	2001.04.12 09:39	X2.0	S19W43	no
13	2001.12.03 19:00	3.0	3+	−32	17.9	505	1.74	2001.11.30 01:00	M3.5	S06E57	no
14[I]	2002.01.27 15:00	3.2	3−	−29	9.0	389	1.42	2002.01.24 03:25	C7.1		no
15	2003.02.01 14:00	4.3	6−	−72	13.1	787	1.83	2003.01.30 10:06 (CME)	DSF	North part of central zone	±
16	2003.10.21 18:00	5.9	6	−61	11.8	744	1.05	2003.10.19 16:29	X1.1	N08E58	–
17	2004.12.27 06:00	2.3	3−	−38	9.9	559	1.25	2004.12.24 2:55	C1.8	S23E45	–
18	2012.05.03 23:00	2.1	3	−8	8.0	334	1.45	2012.04.28 21:48 (CME)	DSF	South part of central zone	–
19	2012.05.30 17:00	2.8	4−	−5	9.9	444	1.17	2012.05.27 4:42	C3.1	S13E57	–
20	2012.07.26 11:00	2.2	2	−22	13.3	403	1.85	2012.07.23 11:21	C2.0	N27E78	no
21	2013.08.24 00:00	3.0	3−	−23	8.8	521	3.04	2013.08.20 8:12 (CME)	DSF	S31W18*	–
22	2013.12.15 13:00	2.7	3−	−24	9.0	501	1.42	2013.12.12 03:11	C4.6	S23W46	no
23[I]	2014.04.05 10:00	2.6	4−	−16	17.6	502	0.89	2014.04.02 13:18	M6.5	N10E62	–
24	2014.04.18 02:00	4.2	4−	−13	10.2	506	1.10	2014.04.14 13:25 (CME)	DSF	Central part of solar disk	+
25	2015.08.25 18:00	4.2	6+	−77	14.2	417	1.70	2015.08.21 19:10	M1.1	S12E26	±
26	2016.06.14 12:00	2.3	6+	−22	14.2	676	1.13	2016.06.11 21:59	C6.5	N14W76	no
27	2016.06.22 05:00	2.3	5−	−11	13.1	425	1.24	2016.06.19 11:44	C1.7	N11W30	no

*Coordinates are taken from cdaw.gsfc.nasa.gov/CME_list/halo/halo.html.

(DSF), therefore the ninth and tenth columns represent "DSF" and clarifications on its location. The last column gives the type of the observed precursor signals, indicating with a minus (−) the predecreases, with a plus (+) the preincreases, and with a plus/minus (±) the events that are connected with both of them (details are given in the section below).

For the early time periods, and also where there were no observations in the ultraviolet and from spacecraft coronagraphs, in order to choose possible solar sources, we relied only on the speed of the solar wind near the Earth and on the coordinates of solar flares. This is why the level of trust for these associations is not high during this period.

Temporal profiles of two typical events selected from Table 2, the first one on 27 January 2002 (without precursor signals) and the second one on 22 May 1999 (with precursor), are presented in the upper and lower portions of Figure 1, respectively. In this figure, temporal profiles of the solar-wind speed and the IMF (upper panels), the CR intensity at 10 GV [A_o] and A_{xy} (middle panels), and the Kp and Dst indices (lower panels) are shown. It is noted that the onset time is defined by the first hour of the IMF increase.

Concerning the first event, its solar source was a C7.1 (GOES class) solar flare on 24 January 2002 at 03:25 UT. The solar-wind velocity and the IMF reached maximum values of 389 km s^{-1} and 9.0 nT near the Earth, respectively (Figure 1; upper diagram; upper panel). The CR equatorial anisotropy one hour before the event onset on 27 January 2002 at 15:00 UT was equal to 1.42% and the FD amplitude was 3.2% at 10 GV (Figure 1; upper diagram; middle panel). This event was not associated with enhanced geomagnetic activity (Figure 1; upper diagram; lower panel).

On the other hand, the source of the interplanetary disturbance of the FD of 22 May 1999 at 19:00 UT is not clearly identified. Only a few weak solar flares were recorded. The maximum value of the solar-wind velocity reached 489 km s^{-1} and the IMF was 8.4 nT (Figure 1; lower diagram; upper panel). The CR decrease was 2.7% at the rigidity of 10 GV and the value of A_{xy} one hour before the onset was 1.83% (Figure 1; lower diagram; middle panel). This FD was also not related to enhanced geomagnetic activity (Figure 1; lower diagram; lower panel).

4. Analysis of Precursors

Examining the total number of events using the RSM and based on the above criteria, 27 FDs were selected for the study of precursors. To confirm the results obtained by this method, temporal profiles of CR intensity provided by twelve individual NMs used in this method of analysis and that recorded both the aforementioned FDs of 27 January 2002 and of 22 May 1999, are presented in Figure 2. These stations are NVBK, MGDN, KERG, INVK, TXBY, YKTK, NEWK, MWSN, APTY, OULU, KIEL, and MOSC. In the left panel of Figure 2, precursor signs of the FD of 27 January 2002 seem not to appear, while in the right panel of the same figure a predecrease before the onset time of the event of 22 May 1999 is observed. We note that in this figure, temporal intervals of more than two days before the onset time of the event have been taken into account to achieve a better distinction between precursory signals and CR variations.

Specifically, in the temporal profiles of the CR intensity of the FD of 27 January 2002 displayed in the left panel of Figure 2, a small CR variation, before the event onset indicated by the vertical line, is observed that is possibly due to the CR diurnal anisotropy. It is a common recurring feature of the CR intensity due to the Earth's daily rotation (Bieber and Chen, 1991; Tezari et al., 2016; Thomas et al., 2017). This variation, confirmed by Fourier analysis as a CR daily variation, does not appear in all of the above individual stations (such

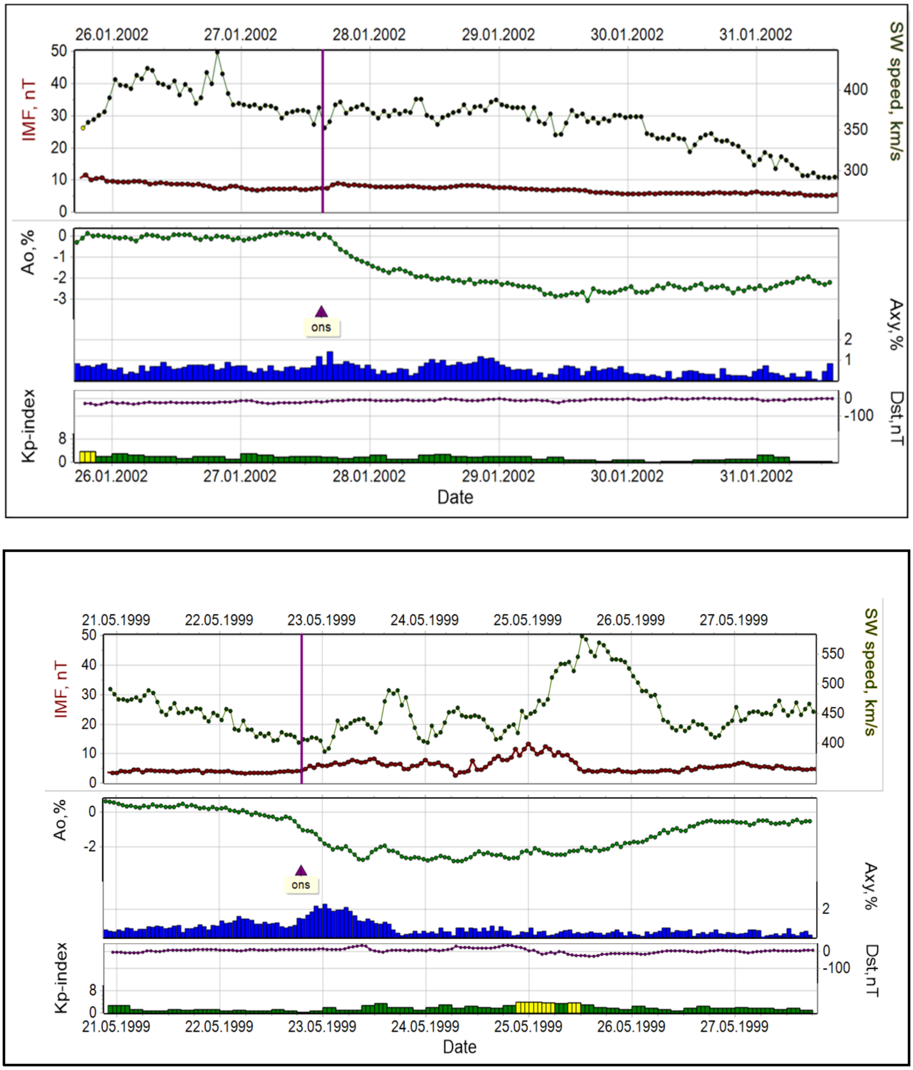

Figure 1 Temporal profiles of the main parameters of the FDs of 27 January 2002 (*upper diagram*) and of 22 May 1999 (*lower diagram*). Each diagram includes the temporal profiles of the solar-wind velocity (*green line*) and the IMF (*red line*) (*upper sub-panels*), of the CR intensity [A_o] at 10 GV (*green line*), and the anisotropy variation on the ecliptic plane [A_{xy}] (*blue histogram*) (*middle sub-panels*) and the geomagnetic indices Dst (*purple line*) and Kp (*histogram*) (*lower sub-panels*). The onset time (ons) is also indicated with the *purple vertical line* and with the *purple triangle*.

as INVK and TXBY) (see below, Figure 3). The existence of a variation before the onset greater than the daily CR in some stations is in the range of statistical error and could not be confirmed as a predecrease. The results of RSM are in agreement with this. Moreover, during the time period of 25 to 31 January 2002 presented in this figure, except for the FD of 27 January studied here, a Forbush effect with an amplitude of about 0.6% is also displayed in some stations two days before, on 25 January 2002. By the next day, the IMF returned

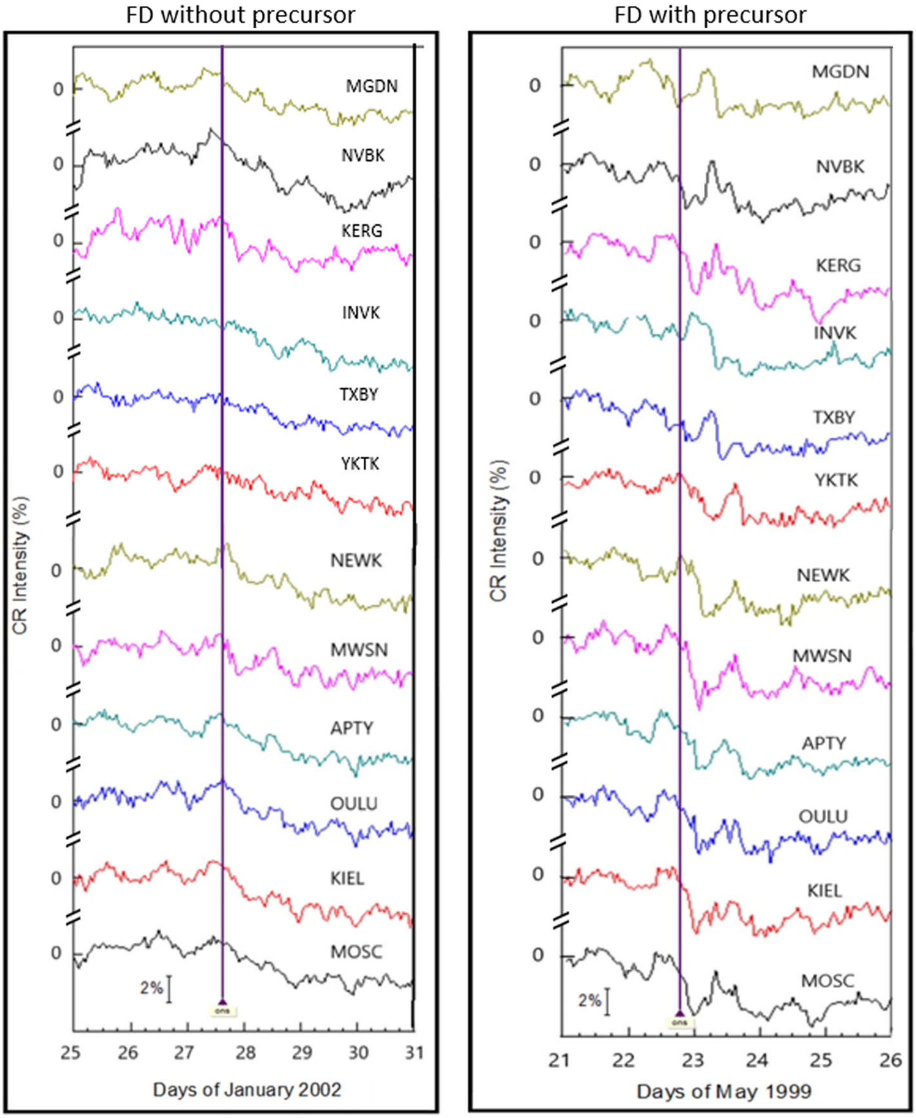

Figure 2 Time–intensity profiles of the FDs of 25 – 31 January 2002 (*left panel*) and of 21 – 26 May 1999 (*right panel*), as they are recorded by twelve common individual NMs**.** The *magenta line* indicates the event onset time, while *the scale is defined at the bottom-left corner*.

to normal levels, so the analysis for precursors of the event on 27 January 2002 could be continued without any problem.

On the other hand, the time–intensity profiles of the FD of 22 May 1999, displayed in the right panel of Figure 2, are a little different. In this case, it is noted that a CR decrease before the event onset (22 May) is observed that is greater than the one observed one day before (21 May) in most of the temporal profiles of NMs (except INVK, MWSN, and MGDN NMs). It is noted that MGDN observed the FD before the indicated onset time. Based on the above, the observed decrease consists of a precursory signal of this event and cannot be characterized as a CR daily variation. During the temporal interval from 21 to 26 May of 1999 presented in the right panel of Figure 2, a series of three FDs is illustrated. In the recovery phase of the first FD starting on 22 May, which is analyzed in this study, a second one is observed around 1200 UT on 23 May. A third one followed on the 25 May.

As is concluded from Figure 2, it is not easy to identify a precursor by using only the NM temporal profile. In this work, in order to obtain more accurate and certain results concerning the existence or not of precursors, RSM is used. CR data from individual NMs from the worldwide network are represented in the same diagram for identifying precursory signals before the onset time of FDs. In this method, the raw data of NMs are used and only changes in the asymptotic longitude of the stations are taken into account. In order to better explain the RSM viewpoint and the possible existence of a precursor, plots of the asymptotic-longitude distribution of CR intensity, as it is recorded by several NMs for a four-day period around the FD of 27 January 2002 (25 – 30 January) and around the one of 22 May 1999 (20 – 24 May), are presented in Figure 3 (upper and lower panels, respectively). First, these plots are created by using simultaneous data from different NM stations. The bubbles on each diagonal ideal line represent hourly data of each station with asymptotic longitude 0° to 360° due to the Earth's rotation with each line corresponding to 24 hours. Hence, in such diagrams, each station is presented in four diagonal lines, one for every day, respectively.

Each NM records CR variations that depend on the station's location and the characteristics of the incoming solar-wind stream. The 180° asymptotic longitude corresponds to the line that connects the Sun with the Earth. Considering the averaged value of the CR intensity, corresponding to a quiet 24-hour period before the event onset, each CR value greater than this is characterized as an increase (yellow bubbles), while a smaller value is considered as a decrease (red bubbles). The size of the bubbles indicates the difference in the CR intensity from the quiet period every hour. The labels on the figures indicate the abbreviation of the stations that recorded a precursor signal.

For the precursor study of the FD on 27 January 2002 by RSM, data from 18 NMs were used. A visualized result of the RSM presenting this FD without a precursor signal is shown in Figure 3 (upper panel). Before the event onset, red bubbles are located in the asymptotic longitudes lower than 180°, while yellow bubbles are above this value. This is due to the diurnal anisotropy of the CR intensity. Before the FD onset, the size of all the bubbles is relatively small. At the onset time, indicated by the abrupt IMF increase, all the bubbles start to become larger and red for all NMs, with a time delay in some of them due to their location. The largest points display the minimum of the FD. The date on the horizontal axis includes 96 hours and focuses on the day before the onset to search for possible precursor existence.

In the FD with a precursory signal (Figure 3, lower panel), the bubbles around 180° before the event onset are different from the previous FD. The bubbles' size a few hours before the onset for several NMs is greater and the asymptotic-longitude ranges, where they appear, change significantly, either by expanding or by being locating in specific longitudes. This indicates a precursor sign, which is classified as predecrease or preincrease, depending on the color of the bubble. A predecrease of CR intensity for the FD on 22 May 1999 is well observed in Figure 3 (lower panel). The asymptotic longitudes of the signal range from 60° to 230° about 26 hours before the event onset. The signal becomes wider close to the onset. Data from fourteen NMs have been studied and eleven of them record this precursor signal (APTY, GSBY, KERG, KIEL, MOSC, NEWK, NVBK, OULU, SNAE, TXBY, and YKTK).

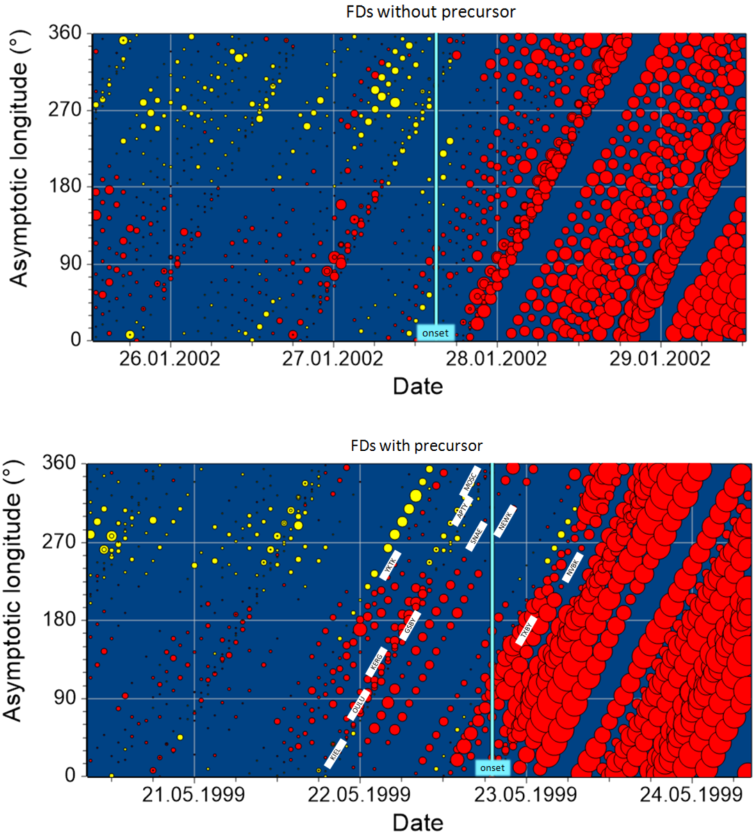

Figure 3 The asymptotic-longitude–time distributions of the FDs of 27 January 2002, in which a precursor signal is not observed (*upper panel*) and of 22 May 1999, in which a predecrease signal is detected (*lower panel*). The *cyan line* indicates the onset of the event. The *labels* indicate the NMs that detected a precursory signal.

5. Results and Discussion

From our analysis, 17 out of 27 selected FD events presented a precursory signal (63% of the events). It is noted that the majority of the studied events (11 out of 17) are recorded during the two recent solar cycles, as in this time period the observations are more accurate and systematic for the solar and interplanetary parameters than in previous cycles. The lack of events during Solar Cycle 22 is due to the existing gaps in the solar-wind and IMF data that obstruct the investigation for possible interesting events at this period.

FDs that are associated with precursors appeared around the descending phases and the minima of the solar cycles. It is also noted that FDs associated with SSC are more usually observed around the maximum and the declining phase of solar activity (Ahluwalia, Ygbuhay, and Duldig, 2009; Lingri et al., 2019). During the solar maximum, solar events occur continuously. Therefore, it is more difficult to distinguish FDs for the study of precursors, since each subsequent FD can start against a disturbed background, which contradicts the conditions for selecting events.

Most FDs present predecrease signals (ten FDs), two FDs have preincrease and six of them present both preincrease and predecrease signals. The time window where a precursor is detected differs between the cases of single and double signals, with the single ones being more long-lasting. Differences are also observed in the asymptotic longitudes where, in both signal cases, the asymptotic longitudes range is narrower than the single precursors. This differentiation in both signal cases has also been recorded at FDs associated with SSC (Lingri et al., 2019) and seems to apply to all the events with both precursory signals.

Usually, the predecreases are explained by the magnetic coupling of the Earth's vicinity with the inner part of the interplanetary disturbance, in which a sufficiently deep FD is observed (Belov et al., 1995; Kudela et al., 2000). In the events considered here, which are mainly associated with eastern CMEs, the mechanism of predecrease is a little different. It can be assumed that the explanation is that the regions of low CR density are wider than those of the interplanetary disturbance.

Preincrease signals are rare due to the absence of shock waves. The front of interplanetary disturbances, as well as the front of shock waves, reflect and accelerate charged particles, especially if the interplanetary disturbance has a sufficiently high velocity and preincreases are recorded (Dorman et al., 1995; Belov, 2008). However, in the cases without an interplanetary shock wave, like those in this study, the solar-wind velocity is generally low and a preincrease is not often observed.

In the next subsections, two specific events with precursor signals are described, and a comparison of FDs with and without SSC during Solar Cycle 24 is performed.

5.1. Forbush Decrease of 10 October 1980

An interesting FD was recorded on 10 October 1980 at 21:00 UT. GOES spacecraft data for the time period of two to three days before the onset of this FD had recorded several powerful solar flares, most of which originated from eastern solar active regions. One of them was an M3.4 flare with coordinates S07E65 on 08 October at 20:21 UT followed by a small solar energetic particle enhancement. Hence, the main body of this ejection diverged quickly and far from the Parker spiral connecting the Sun and the Earth, with only a small part of it eventually reaching the Earth. The solar-wind velocity that was recorded in the interplanetary space close to Earth was not so high (579 $\mathrm{km\,s^{-1}}$) but the IMF reached the value of 14 nT and created a small FD with an amplitude of 2.7% at 10 GV, as well as an intense geomagnetic storm.

Studying this event for precursors, both predecrease and preincrease are observed (Figure 4). The predecrease started about 22 hours before the onset. In the beginning, it was located in a range of 100° and 170° asymptotic longitudes. After 8 hours, a preincrease signal was observed from 180° to 280° asymptotic longitudes and lasted for the next 10 hours. In the midtime, the predecrease started to expand to smaller longitudes and to reduce the upper longitude from 170° to 150° degrees. From the twenty NMs, whose data are studied, greater predecrease, in these asymptotic longitudes, is recorded by DPRV, DRHM, GSBY, KIEL, LEED, NEWK, SNAE, and YKTK NM stations. On the contrary, APTY, INVK, KERG, NRLK, NVBK, OULU, SVER, and TXBY NM stations recorded a preincrease signal.

Finally, during the final 4 hours before the onset, there was only the predecrease signal, which had already covered a wide range of asymptotic longitudes (0 – 150°). It is unexpected and atypical for an FD with an amplitude of only 2.7% at 10 GV to have large and long-lasting precursory signals. A possible reason for this may be that the solar source was eastern and the stream propagated quickly far from the Earth. If our location was closer to the center of the eruption the recorded event would be greater.

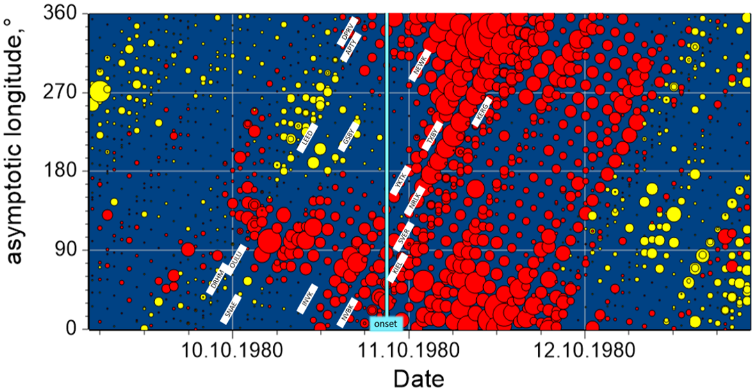

Figure 4 The asymptotic-longitude temporal distribution of the FD of 10 October 1980. The labels indicate the sixteen NM stations that detected predecrease and/or preincrease precursory signals.

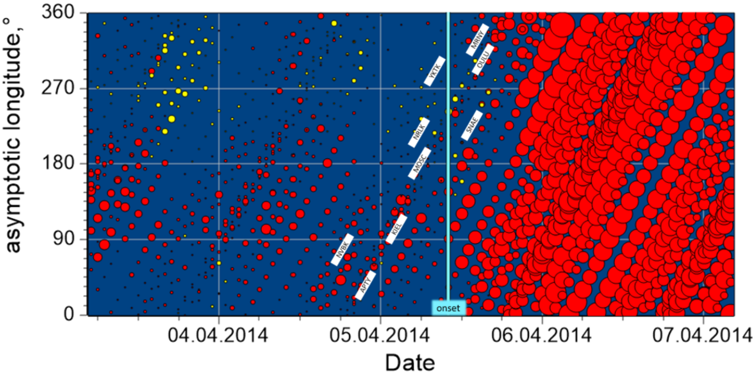

Figure 5 The asymptotic-longitude–time distribution of the FD on 05 April 2014. The labels indicate the nine NMs that detected a predecrease precursory signal.

5.2. Forbush Decrease of 05 April 2014

On 02 April 2014, during the second peak of Solar Cycle 24, an M6.5 flare (with coordinates N10E62) was seen in Active Region 12030. In the same time period, a halo CME was observed by the SOHO spacecraft. It was a major CME with its linear velocity reaching a value of 1471 $\mathrm{km\,s^{-1}}$, but it did not strongly affect the Earth's magnetosphere. Although the solar-wind velocity reached a maximum value of 505 $\mathrm{km\,s^{-1}}$ and the IMF reached the value of 17.6 nT, no shock was recorded by the ACE spacecraft, but the disturbance was observed in CR intensity, as an FD on 05 April 2014 at 10:00 UT, with an amplitude equal to 2.6% at the rigidity of 10 GV.

A typical predecrease before the onset of the main phase of the event is observed (Figure 5). The predecrease started about 18 hours before the onset, with an asymptotic-longitude range between 80° and 180°. It is characterized as a typical precursor as its shape is similar to most detected predecreases. It was recorded by 9 (APTY, KIEL, MRNY, MOSC, NRLK, OULU, NVBK, SNAE, and YKTK) out of 17 NMs.

Table 3 Values of the various parameters of FDs with and without SSC association during Solar Cycle 24.

FD Parameters	Range		Average values	
	FDs with SSC	FDs without SSC	FDs with SSC	FDs without SSC
FD Amplitude [%] at 10 GV	2.5 to 6.4	2.0 to 4.2	4.3±0.3	3.2±0.3
Dst index [nT]	−139 to −22	−77 to −5	(−70.3)±10.9	(−24)±11.0
Kp index	3+ to 7+	3− to 6+	6−±0+	4−±0+
IMF [nT]	7.6 to 40.1	8.0 to 17.6	19.5±2.1	11.5±1.5
V_{sw} [km s^{-1}]	404 to 727	334 to 521	575±28	454±29

5.3. FDs with and without SSC

During Solar Cycle 24 by comparing the events with SSC (16 events, published by Lingri et al., 2019) to the ones without SSC of this study (6 out of 17), interesting results are obtained. The different ranges of some crucial parameters between the two event categories are presented in Table 3. The compared parameters are given in the first column, the ranges of these parameters for both categories are presented in the second and third column, respectively, while their averaged values for events with and without SSC are given in the last two columns, respectively. The FD amplitude ranges from 2% to 4.2% for FDs without SSC association with a mean value equal to 3.2% at the rigidity of 10 GV, while the range of the FDs with SSC fluctuates from 2.5% to 6.4%, with the mean value at 4.3% at 10 GV. This means that the FDs with associated SSC present, on average, greater amplitudes. The variability of the geomagnetic indices is more intense in FDs with SSCs since most of them are connected with moderate and intense storms. The values of the IMF and solar-wind velocity maximum are in most cases greater for the FDs with SSC association. As was expected, the average values of these parameters seem to be greater in the case of the events associated with SSC.

6. Conclusions

In this work, 27 FDs that occurred during the last fifty years (1969 – 2019) covering almost five solar cycles (20 – 24), with amplitude greater than 2% and without an interplanetary shock wave near the Earth are studied for precursors. Most of the examined events are observed during the two recent Solar Cycles 23 and 24.

The main conclusions of this study are:

- CR precursors also exist in FDs without SSC.
- The majority (63%) of the examined events without SSC present a precursory signal.
- Precursors determined before a FD without SSC onset time are anisotropic phenomena and can be observed as predecreases or/and preincreases. This result is in accordance with previous studies concerning FDs with SSC (e.g. Belov et al., 1995; Kudela et al., 2000; Leerungnavarat, Ruffolo, and Bieber, 2003).
- In the case of FDs without SSC, predecreases and both signals are more often observed than preincreases.
- The solar-erupting events that produced FDs without SSC often originated from active regions located on the eastern part of the solar disk.

It should be emphasized that the existence of precursors before the onset of FDs could be observed ahead of the interplanetary disturbances fronts that do not create shock waves. The use of the RSM method seems to be more suitable for the study of the precursor existence in comparison to the study based on the observations of individual stations.

Acknowledgments Special thanks are due to the PIs of the NM stations (www.nmdb.eu) for kindly providing the CR data used in this study in the frame work of the *European High-resolution Real-time Neutron Monitor Database* funded under the European Union's FP7 Program (contract no. 213007). Thanks are due to the IZMIRAN/FEID, ACE/*Wind*, OMNI, and NOAA data centers. Thanks are due to the anonymous reviewers for valuable suggestions for significantly improving this work.

Funding This research was supported by the Hellenic Foundation for Research and Innovation (HFRI) and the General Secretariat for Research and Technology (GSRT), under the HFRI PhD Fellowship grant (GA. no. 14492). For this study, M. Abunina and A. Belov have been supported by the Russian Science Foundation under grant 20-72-10023, and A. Abunin by the Russian Foundation of Basic Research under grant 18-52-34004.

Data Availability The datasets generated during and/or analyzed during the current study are available from the corresponding author on reasonable request.

Declarations

Conflict of Interest The authors indicate that there is no conflict of interest.

References

Abunin, A.A., Abunina, M.A., Belov, A.V., Gaidash, S.P., Eroshenko, E.A., Pryamushkina, I.I., Trefilova, L.A., Gamza, E.I.: 2019, Database capabilities for studying Forbush-effects and interplanetary disturbances. In: Lagutin, A. (ed.) *26th Extended European Cosmic Ray Symposium*, *J. Phys.* **CS-1181**, ID012062. DOI

Abunina, M.A., Belov, A.V., Eroshenko, E.A., Abunin, A.A., Yanke, V.G., Melkumyan, A.A., Shlyk, N.S., Pryamushkina, I.I.: 2020, Ring of Stations Method in Cosmic Rays Variations Research. *Solar Phys.* **295**, 69. DOI.

Ahluwalia, H.S., Ygbuhay, R.C., Duldig, M.L.: 2009, Two intense Forbush decreases of solar activity cycle 22. *Adv. Space Res.* **44**, 58. DOI.

Asipenka, A.S., Belov, A.V., Eroshenko, E.A., Klepach, E.G., Oleneva, V.A., Yanke, V.G.: 2009, Interactive database of cosmic ray anisotropy (DB-A10). *Adv. Space Res.* **43**, 708. DOI.

Belov, A.: 2008, Forbush effects and their connection with solar, interplanetary and geomagnetic phenomena. In: Gopalswamy, N., Webb, D. (eds.) *Universal Heliophysical Processes, Proc. IAU Symp.* **257**, Cambridge Univ. Press, Cambridge, 439. DOI.

Belov, A.V., Dorman, L.I., Eroshenko, E.A., Iucci, N., Villoresi, G., Yanke, V.G.: 1995, Search for predictors of Forbush decreases. In: Iucci, N., Lamanna, E. (eds.) *Proc. 24th ICRC, Rome*, *Internat. Union Pure Appl. Phys.*, **4**, 888.

Belov, A.V., Bieber, J.W., Eroshenko, E.A., Evenson, P., Pyle, R., Yanke, V.G.: 2003, Cosmic ray anisotropy before and during the passage of major solar wind disturbances. *Adv. Space Res.* **31**, 919. DOI.

Belov, A.V., Abunina, M.A., Abunin, A.A., Eroshenko, E.A., Oleneva, V.A., Yanke, V.G.: 2017a, Cosmic ray vector anisotropy and local characteristics of the interplanetary medium. *Geomagn. Aeron.* **57**, 389. DOI.

Belov, A.V., Abunina, M.A., Abunin, A.A., Eroshenko, E.A., Oleneva, V.A., Yanke, V.G.: 2017b, Vector anisotropy of cosmic rays in the beginning of Forbush effects. *Geomagn. Aeron.* **57**, 541. DOI.

Belov, A., Eroshenko, E., Yanke, V., Oleneva, V., Abunin, A., Abunina, M., Papaioannou, A., Mavromichalaki, H.: 2018, The global survey method applied to ground-level cosmic ray measurements. *Solar Phys.* **293**, 68. DOI.

Belov, A., Abunin, A., Eroshenko, E., Abunina, M., Yanke, V., Oleneva, V.: 2019, Virtual laboratory for the comprehensive analysis of Forbush-effects and interplanetary disturbances. *VarSITI Newsl.* **21**, 1. newserver.stil.bas.bg/varsiti//newsL/VarSITI_Newsletter_Vol21_high_reso.pdf.

Bieber, J.W., Chen, J.L.: 1991, Cosmic ray diurnal anisotropy, 1936 – 88: Implications for drift and modulation theories. *Astrophys. J.* **372**, 301. DOI.

Cane, H.V.: 2000, Coronal mass ejections and Forbush decreases. *Space Sci. Rev.* **93**, 55. DOI.

Dorman, L.I.: 2005, Space weather and dangerous phenomena on the Earth: principles of great geomagnetic storms forcasting by online cosmic ray data. *Ann. Geophys.* **23**, 2997. DOI.

Dorman, L.I., Villoresi, G., Belov, A.V., Eroshenko, E.A., Iucci, N., Yanke, V.G., Yudakhin, K.F., Bavassano, B., Ptitsyna, N.G., Tyasto, M.I.: 1995, Cosmic-ray forecasting features for big Forbush decreases. *Nucl. Phys. B, Proc. Suppl.* **39**, 136. DOI.

Dumbović, M., Vršnak, B., Guo, J., Heber, B., Dissauer, K., Carcaboso, F., Temmer, M., Veronig, A., Podladchikova, T., Möstl, C., Amerstorfer, T., Kirin, A.: 2019, Evolution of Coronal Mass Ejections and the Corresponding Forbush Decreases: Modeling vs. Multi-Spacecraft Observations. *Solar Phys.* **295**, 104. DOI.

Forbush, S.: 1938, On cosmic-ray effects associated with magnetic storms. *Terr. Magn. Atmos. Electr.* **43**, 203. DOI.

Forbush, S.E.: 1954, World-wide cosmic-ray variations, 1937 – 1952. *J. Geophys. Res.* **59**, 525. DOI.

Hofer, M.Y., Fluckiger, E.O.: 2000, Cosmic ray spectral variations and anisotropy near Earth during the March 24, 1991, Forbush decrease. *J. Geophys. Res.* **105**, 23085. DOI.

Iucci, N., Parisi, M., Storini, M., Villoresi, G.: 1979, High-speed solar-wind streams and galactic cosmic ray modulation. *Nuovo Cimento C* **2**, 421. DOI.

Jacklyn, R.M., Duggal, S.P., Pomerantz, M.A.: 1969, Solar Diurnal Anisotropy of Cosmic Rays. *Nature* **223**, 5206, 601. DOI.

Janvier, M., Winslow, R.M., Good, S., Bonhomme, E., Démoulin, P., Dasso, S., Möstl, C., Lugaz, N., Amerstorfer, T., Soubrié, E., Boakes, P.D.: 2019, Generic magnetic field intensity profiles of interplanetary coronal mass ejections at Mercury, Venus, and Earth from superposed epoch analyses. *J. Geophys. Res.* **124**, 812. DOI.

Kudela, K., Storini, M.: 2006, Possible tools for space weather issues from cosmic ray continuous records. *Adv. Space Res.* **37**, 1443. DOI.

Kudela, K., Storini, M., Hofer, M.Y., Belov, A.V.: 2000, Cosmic Rays in Relation to Space Weather. *Space Sci. Rev.* **93**, 153. DOI.

Kuwabara, T., Bieber, J.W., Clem, J., Evenson, P., Pyle, R., Munakata, K., Yasue, S., Kato, C., Akahane, S., Koyama, M., Fujii, Z., Duldig, M.L., Humble, J.E., Silva, M.R., Trivedi, N.B., Gonzalez, W.D., Schuch, N.J.: 2006, Real-time cosmic ray monitoring system for space weather. *Space Weather* **4**, S08001. DOI.

Leerungnavarat, K., Ruffolo, D., Bieber, J.W.: 2003, Loss cone precursors to Forbush decreases and advance warning of space weather effects. *Astrophys. J.* **593**, 587. DOI.

Lingri, D., Mavromichalaki, H., Belov, A., Eroshenko, E., Yanke, V., Abunin, A., Abunina, M.: 2016, Forbush decreases during the DeepMin and MiniMax of Solar Cycle 24. In: Chiavassa, A. (ed.) *XXV ECRS 2016 Proceedings – eConf C16-09-04.3*. arXiv.

Lingri, D., Mavromichalaki, H., Belov, A., Abunina, M., Eroshenko, E., Abunin, A.: 2019, An Extended Study of the Precursory Signs of Forbush Decreases: New Findings over the Years 2008 – 2016. *Solar Phys.* **294**, 70. DOI.

Lockwood, J.A.: 1971, Forbush Decreases in the Cosmic Radiation. *Space Sci. Rev.* **12**, 658. DOI.

Mavromichalaki, H., Papaioannou, A., Plainaki, C., Sarlanis, C., Souvatzoglou, G., Gerontidou, M., Papailiou, M., Eroshenko, E., Belov, A., Yanke, V., Flückiger, E.O., Bütikofer, R., Parisi, M., Storini, M., Klein, K.-L., Fuller, N., Steigies, C.T., Rother, O.M., Heber, B., Wimmer-Schweingruber, R.F., Kudela, K., Strharsky, I., Langer, R., Usoskin, I., Ibragimov, A., Chilingaryan, A., Hovsepyan, G., Reymers, A., Yeghikyan, A., Kryakunova, O., Dryn, E., Nikolayevskiy, N., Dorman, L., Pustil'nik, L.: 2011, Applications and usage of the real-time Neutron Monitor Database. *Adv. Space Res.* **47**, 2210. DOI.

Melkumyan, A.A., Belov, A.V., Abunina, M.A., Abunin, A.A., Eroshenko, E.A., Yanke, V.G., Oleneva, V.A.: 2019, Comparison between statistical properties of Forbush decreases caused by solar wind disturbances from coronal mass ejections and coronal holes. *Adv. Space Res.* **63**, 1100. DOI.

Melkumyan, A.A., Belov, A.V., Abunina, M.A., Abunin, A.A., Eroshenko, E.A., Oleneva, V.A., Yanke, V.G.: 2021, Solar wind temperature-velocity relationship over the last five solar cycles and Forbush decreases associated with different types of interplanetary disturbance. *Mon. Not. Roy. Astron. Soc.* **500**, 2786. DOI.

Munakata, K., Bieber, J.W., Yasue, S., Kato, C., Koyama, M., Akahane, S., Fujimoto, K., Fujii, Z., Humble, J.E., Duldig, M.L.: 2000, Precursors of geomagnetic storms observed by the muon detector network. *J. Geophys. Res.* **105**, 27457. DOI.

Nagashima, K., Fujimoto, K., Sakakibara, S., Morishita, I., Tatsuoka, R.: 1992, Local-time-dependent pre-IMF-shock decrease and post-shock increase of cosmic rays, produced respectively by their IMF-collimated outward and inward flows across the shock responsible for Forbush decrease. *Planet. Space Sci.* **40**, 1109. DOI.

Nagashima, K., Sakakibara, S., Fujimoto, K., Fujji, Z., Ueno, H.: 1993, Local-time-dependent precursory decrease of cosmic rays, in front of Forbush-decrease-associated IMF shock wave, observed on September 9, 1992. In: Leahy, D.A., Hicks, R.B., Venkatesan, D. (eds.) *Proc. 23rd ICRC, Calgary*, **3**, World Scientific, Singapore, 711.

Okike, O., Collier, A.B.: 2011, A multivariate study of Forbush decrease simultaneity. *J. Atmos. Solar-Terr. Phys.* **73**, 796. DOI.

Papailiou, M., Mavromichalaki, H., Belov, A., Eroshenko, E., Yanke, V.: 2012a, Precursor effects in different cases of Forbush decreases. *Solar Phys.* **276**, 337. DOI.

Papailiou, M., Mavromichalaki, H., Belov, A., Eroshenko, E., Yanke, V.: 2012b, The asymptotic longitudinal cosmic ray intensity distribution as a precursor of Forbush decreases. *Solar Phys.* **280**, 641. DOI.

Papailiou, M., Mavromichalaki, H., Abunina, M., Belov, A., Eroshenko, E., Yanke, V., Kryakunova, O.: 2013, Forbush Decreases Associated with Western Solar Sources and Geomagnetic Storms: A Study on Precursors. *Solar Phys.* **283**, 557. DOI.

Richardson, I.G.: 2004, Energetic Particles and Corotating Interaction Regions in the Solar Wind. *Space Sci. Rev.* **111**, 267. DOI.

Ruffolo, D., Bieber, J.W., Everson, P., Pyle, R.: 1999, Precursors to Forbush Decreases and Space Weather Prediction. In: Kieda, D., Salamon, M., Dingus, B. (eds.) *Proc. 26th ICRC, Salt Lake City*, *Internat. Union Pure App. Phys.*, **6**, 440.

Russell, C.T., Mulligan, T.: 2002, On the magnetosheath thicknesses of interplanetary coronal mass ejections. *Planet. Space Sci.* **50**, 527. DOI.

Simpson, J.A.: 2000, The Cosmic Ray Nucleonic Component: The Invention and Scientific Uses of the Neutron Monitor. *Space Sci. Rev.* **93**, 11. DOI.

Tezari, A., Mavromichalaki, H., Katsinis, D., Kanellakopoulos, A., Kolovi, S., Plainaki, C., Andriopoulou, M.: 2016, Latitudinal and longitudinal dependence of the cosmic ray diurnal anisotropy during 2001-2014. *Ann. Geophys.* **34**, 1053. DOI.

Thomas, S., Owens, M., Lockwood, M., Owen, C.: 2017, Decadal trends in the diurnal variation of galactic cosmic rays observed using neutron monitor data. *Ann. Geophys.* **35**, 825. DOI.

Tortermpun, U., Ruffolo, D., Bieber, J.W.: 2018, Galactic cosmic-ray anisotropy during the Forbush decrease starting 2013 April 13. *Astrophys. J. Lett.* **852**, L26. DOI.

Väisänen, P., Usoskin, I., Mursula, K.: 2021, Seven Decades of Neutron Monitors (1951 – 2019): Overview and Evaluation of Data Sources. *J. Geophys. Res. Space Phys.* **126**, e28941. DOI.